NASA Technical Paper 3335

April 1993

Analysis of the Staging Maneuver and Booster Glideback Guidance for a Two-Stage, Winged, Fully Reusable Launch Vehicle

J. Christopher Naftel
and Richard W. Powell

NASA

NASA Technical Paper 3335

1993

Analysis of the Staging Maneuver and Booster Glideback Guidance for a Two-Stage, Winged, Fully Reusable Launch Vehicle

J. Christopher Naftel
and Richard W. Powell
Langley Research Center
Hampton, Virginia

National Aeronautics and Space Administration
Office of Management
Scientific and Technical Information Program

Contents

Nomenclature

A_a	axial acceleration, g units
A_n	normal acceleration, g units
b	reference wingspan (measured at fuselage), ft
$C_{D,\text{nom}}$	nominal drag coefficient, $\text{Drag}/q_\infty S_{\text{ref}}$
$C_{L,\text{nom}}$	nominal lift coefficient, $\text{Lift}/q_\infty S_{\text{ref}}$
c	reference wing chord (measured at fuselage), ft
GRAM	Global Reference Atmospheric Model
g	acceleration due to gravity ($1g \approx 32.174$ ft/sec^2)
HAC	heading alignment cylinder
h	altitude, ft
$\dot{h}$	altitude derivative with respect to time, ft/sec
I_{sp}	vacuum specific impulse, sec
I_{xx}, I_{yy}, I_{zz}	moments of inertia about body frame, slug-ft^2
KSC	Kennedy Space Center
K_{qr}	pitch rate gain, sec
$K_{\alpha e}$	angle-of-attack error gain
$K_{\alpha d5}$	angle-of-attack displacement gain of phase 5
$K_{\alpha d6}$	angle-of-attack displacement gain of phase 6
$K_{\alpha r5}$	angle-of-attack rate gain of phase 5, sec
$K_{\alpha r6}$	angle-of-attack rate gain of phase 6, sec
$K_{\phi d5}$	roll-angle displacement gain of phase 5, deg/ft
$K_{\phi r5}$	roll-angle rate gain of phase 5, deg-sec/ft
L/D	lift-to-drag ratio
L_{ref}	reference vehicle length, ft
M	Mach number
NEP	nominal entry point
q	pitch rate, deg/sec
q_∞	dynamic pressure, psf
S_{ref}	reference wing area, ft^2
SRB	solid rocket booster
SSSS	Space Shuttle Separation Simulation
t	time, sec
t_i	initial time, sec
V	atmospheric relative velocity, ft/sec
W_{EW}	east-west wind component (wind from west, positive), ft/sec

W_{NS}	north-south wind component (wind from south, positive), ft/sec
WP1	way point 1
WP2	way point 2
X, Y, Z	reference body frames (origin at vehicle nose), ft
X_{cg}, Y_{cg}, Z_{cg}	center of gravity in X, Y, and Z body frames, respectively, ft
X_{rt}, Y_{rt}	vehicle X and Y positions relative to runway threshold, ft
$\dot{X}_{rt}, \dot{Y}_{rt}$	vehicle X and Y velocities relative to runway threshold, ft/sec
α	angle of attack, deg
α_c	commanded angle of attack, deg
α_i	initial angle of attack, deg
α_S	angle of attack at staging initiation, deg
γ	atmospheric relative flight-path angle, deg
γ_{ref}	reference atmospheric relative flight-path angle, deg
γ_0	constant term in γ_{ref} polynomial, deg
γ_1	linear term in γ_{ref} polynomial, deg/ft
γ_2	quadratic term in γ_{ref} polynomial, deg/ft^2
γ_3	cubic term in γ_{ref} polynomial, deg/ft^3
δ_e	elevon deflection (positive with trailing edge down), deg
$\delta_{e,c}$	commanded elevon deflection, deg
$\delta_{e,i}$	initial elevon deflection, deg
δ_p	pitch gimbal angle on engines (positive up), deg
θ_R	angle between orbiter and booster at release of orbiter from rear strut, deg
$\ddot{\theta}$	pitch acceleration, deg/sec^2
ρ	atmospheric density, slugs/ft^3
ρ_{76}	1976 U.S. Standard Atmospheric density, slugs/ft^3
σ	standard deviation
ϕ	roll angle, deg
ϕ_c	geocentric latitude, deg
ϕ_i	initial roll angle, deg

A dot over a symbol denotes the derivative with respect to time.

Summary

A staging technique and a booster glideback guidance algorithm have been developed for a two-stage, parallel-burn, winged, vertical-takeoff launch system. When the launch system reaches a Mach number of 3, the booster is staged and glides to a horizontal landing at a launch site runway. The staging maneuver and the booster glideback guidance, which are two major design issues for this class of vehicle, are presented in this report.

The staging maneuver is the first design issue analyzed in this report. Initially, a staging maneuver is modeled in which the orbiter is released from both the forward and rearward attachment struts on the booster simultaneously. Using this technique, the booster immediately pitches up into the orbiter. Further analysis shows that if the orbiter is released from the forward attachment strut, the booster pivots about the rearward attachment struts. If the orbiter is then released from the rearward attachment struts after a specified rotation, the booster is able to execute a separation maneuver while avoiding contact with the orbiter and the plumes from the orbiter engines. The booster is controlled aerodynamically during the separation maneuver and does not require a reaction control system.

The second design issue analyzed is the unpowered glideback of the booster to a launch site runway after the staging maneuver is completed. A guidance algorithm is developed for a nominal glideback maneuver using a three-degrees-of-freedom trajectory simulation. The guidance algorithm is tested using off-nominal atmospheric, staging, and booster aerodynamic characteristics. While experiencing each of these off-nominal conditions, the booster is able to touch down on the launch site runway within acceptable distance and descent rate margins.

Introduction

Recent studies of launch vehicles that are intended as follow-ons to the current Space Shuttle launch system have included a two-stage, winged, fully reusable, vertical-takeoff, rocket launch vehicle concept (refs. 1–4). This concept incorporates an unmanned booster that stages from a manned orbiter at a Mach number of 3 and glides back unpowered to the launch site area where it lands horizontally on a runway. A verification of the staging maneuver and booster glideback is critical to demonstrating the feasibility of this two-stage concept. These issues are addressed in-depth for the first time in this report.

Several factors combine to make this staging maneuver at a Mach number of 3 more complicated than the staging maneuver for any vehicle that has flown to date. These factors include the following: (1) both the orbiter and booster are winged, (2) the launch vehicle is a parallel system with the booster attached to the underside of the orbiter, and (3) the dynamic pressure is relatively high during this maneuver.

Staging for this vehicle was set at a Mach number of 3 for two major reasons. The first reason is that this is the highest Mach number that allows an unpowered return to the launch site with adequate performance reserves (ref. 5). This unpowered return eliminates the need for an airbreathing propulsion subsystem on the booster and eliminates the associated maintenance and checkout of the subsystem before each launch. The second reason is that if staging occurs at a higher Mach number, the booster would experience sufficient aerodynamic heating to require a dedicated thermal protection system (ref. 1).

Description of Launch Vehicle

Characteristics of Ascent Configuration

The concept of the launch vehicle analyzed in this investigation is shown in figure 1. Table 1 shows the major characteristics of each stage. The vehicle is composed of an unmanned booster and a manned orbiter. Both the booster and orbiter use identical liquid hydrogen/liquid oxygen rocket engines for development and operational cost reduction. During the boost phase, the orbiter uses propellant that is supplied from the booster tanks. After staging, the orbiter uses propellant supplied from its internal tanks. The containerized payload is carried on the back of the orbiter in an external canister arrangement. Access to the payload canister is through a tunnel leading from the forward crew cabin. Aerodynamic fairings cover the access tunnel and payload canister. The orbiter is connected to forward and rearward attachment struts that are fixed on the top of the booster fuselage (fig. 2). The rearward attachment struts have a pivot linkage that allows for a rotation between the booster and orbiter upon release of the forward attachment strut.

The mission scenario is shown in figure 3. For this analysis, the launch pad is assumed to be a modified Space Shuttle launch pad at the Kennedy Space Center (KSC). The details of the nominal ascent trajectory are discussed in a later section entitled "Nominal Ascent Trajectory." The orbiter is sized to deliver up to 20 000 lb of payload to a 220-n.mi. circular orbit that is inclined 28.5°, which is the reference space station orbit. Both the booster and orbiter are designed to land horizontally at the KSC Shuttle orbiter landing strip at the completion of their missions.

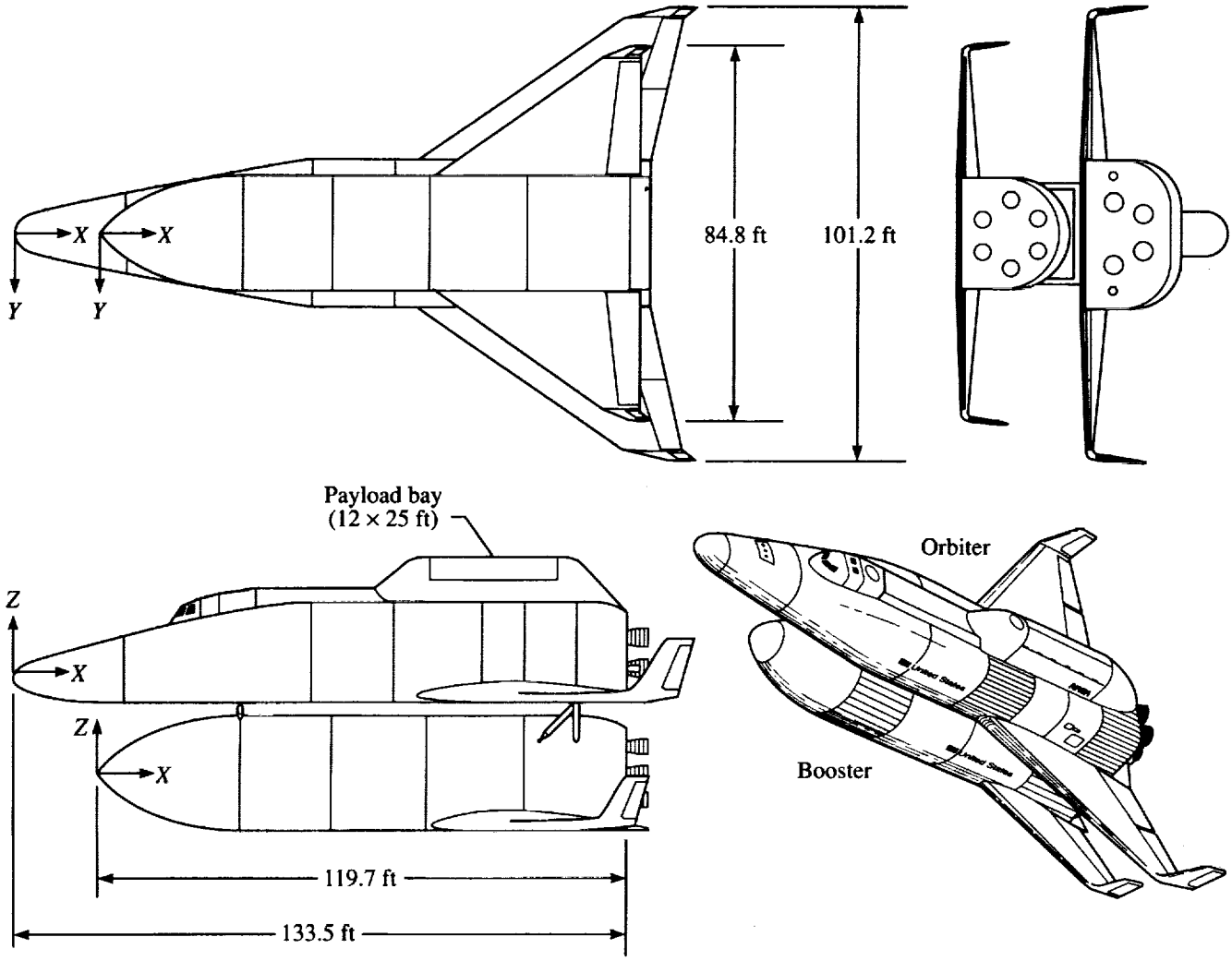

Figure 1. Two-stage, fully reusable concept.

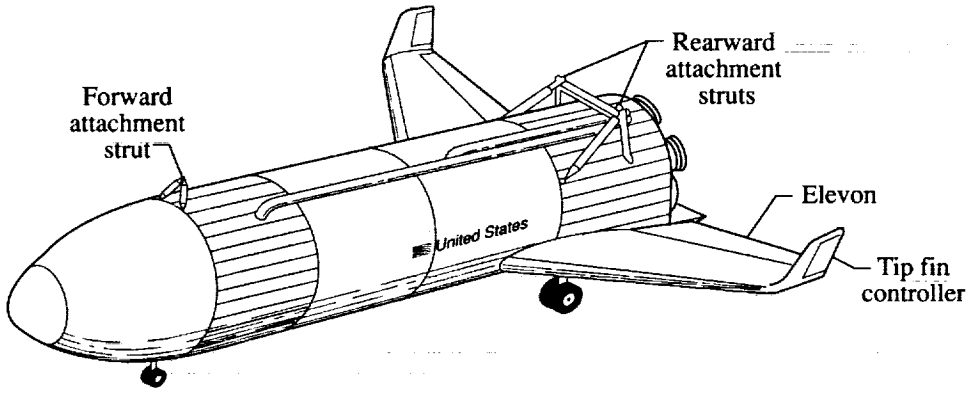

Figure 2. Attachment struts and control surfaces of booster.

Table 1. Characteristics of Orbiter and Booster

Characteristic	Orbiter	Booster
Gross weight, lb	1 186 872	960 636
Dry weight, lb	152 971	107 362
Number of engines	4	6
Single engine vacuum thrust, lb	352 000	352 000
Engine I_{sp}, sec	438	438
Single engine exit area, ft^2	34.3	34.3
S_{ref}, ft^2	3722.6	3291.2
L_{ref}, ft	133.5	119.7
c (measured at fuselage), ft	50.2	43.5
b, ft	101.2	84.8

Characteristics of Booster

The aerodynamic data for the booster are based on a wind tunnel analysis of a similar vehicle that is presented in reference 6. The booster control surfaces include elevons and tip fin controllers (fig. 2). The elevons, which have deflection limits between $-30°$ and $20°$, are used for both pitch and roll control by being differentially deflected so that they can function as both elevators and ailerons. The tip fin controllers, which have deflection limits between $-60°$ and $60°$, are used to control sideslip angle and can function as a speed brake. The booster wings are designed to accommodate a normal force that is 2.5 times the booster landed weight. The landing gear on the booster is designed for a sideslip angle limit between $-3°$ and $3°$ and a maximum descent rate of 3 ft/sec at touchdown.

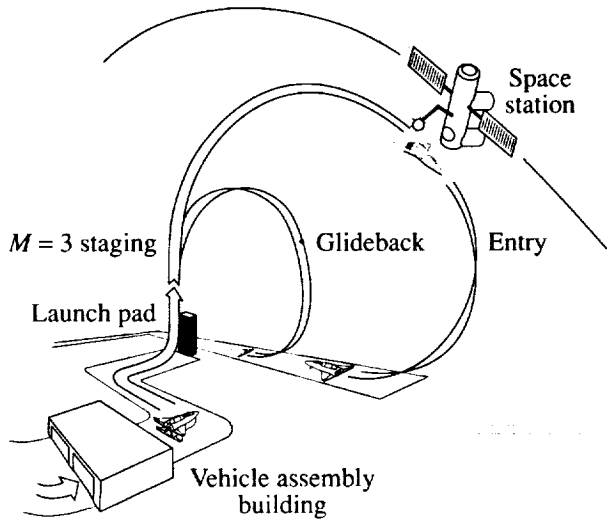

Figure 3. Mission scenario for two-stage, fully reusable concept.

Computational Tools

Space Shuttle Separation Simulation Program

The separation trajectories in this study were generated with the Space Shuttle Separation Simulation (SSSS) program (ref. 7). The SSSS program computes the kinematics of separation in six rigid-body degrees of freedom for a core vehicle (orbiter) and three rigid-body degrees of freedom for up to five auxiliary components (boosters). The equations of motion used in the SSSS program are written about the body axes of the core and each auxiliary. For the core vehicle (with or without auxiliaries attached), the three translational and three rotational equations of motion are integrated. For each auxiliary (when detached from the core), the translational equations in the X and Z body frames and the rotational equation about the Y-axis are integrated. The separation distances and rotations for each auxiliary, relative to the core vehicle, are calculated during the separation trajectory.

Program To Optimize Simulated Trajectories

The ascent and glideback trajectories were generated with the three-degrees-of-freedom version of the Program To Optimize Simulated Trajectories (POST). (See ref. 8.) The POST program deals with generalized point mass, discrete parameter targeting, and optimization with the capability of targeting and optimizing trajectories for a powered or unpowered vehicle near a rotating oblate planet. POST is an event-oriented trajectory program that can be used to analyze ascent, on-orbit, entry, and atmospheric trajectories. Any calculated variable in POST can be optimized while being subjected to a combination of both equality and inequality constraints.

POST was used in a targeting and optimization mode for the development of the nominal ascent trajectory. After several modifications were made to POST for this study, it was used in a simulation mode for the booster glideback trajectories. These modifications included the addition of the closed-loop guidance algorithm that was developed for the glideback of the booster to the launch site runway, the addition of the booster aerodynamic data base, and the addition of the numerous atmospheres and wind profiles that were used to evaluate the guidance algorithm. For the glideback trajectories, the booster was trimmed in pitch with the elevons using the static trim option in POST.

Global Reference Atmosphere Model

The Global Reference Atmosphere Model (GRAM) was used to model the atmospheres for the evaluation of the booster glideback guidance algorithm (ref. 9). The GRAM is an engineering model atmosphere that includes mean values for density, temperature, pressure, and wind components, in addition to random perturbation profiles for density variations along a specified trajectory (ref. 10). The atmospheric data are a function of latitude, longitude, altitude, and day of the year. The random perturbation profile feature allows for the simulation of a large number of realistic density profiles along the same trajectory through the atmosphere, but with realistic peak perturbation values. The atmospheres developed for this study, using GRAM, will be presented in a later section entitled "Analysis of Booster Glideback Guidance."

Nominal Ascent Trajectory

A detailed discussion of the ascent trajectory guidance and flight control issues for the launch configuration in this study can be found in reference 11. The launch site is assumed to be a modified Space Shuttle launch pad at the Kennedy Space Center. The launch vehicle has a maximum dynamic pressure constraint of 800 psf, a maximum axial acceleration constraint of $3g$, and a wing normal-force constraint equal to 2.5 times the dry weight of each stage. The angle of attack at staging ($-1.7°$) was determined by the staging maneuver analysis, which will be discussed in a later section entitled "Analysis of Staging Maneuver." A description of the optimum constrained ascent trajectory follows.

As shown in figure 4, the orbiter reaches its initial orbit 438 sec after launch at an altitude of 303 800 ft, an inertial velocity of 25 844 ft/sec, and an inclination of 28.5°. The orbiter is designed to deliver up to 20 000 lb of payload to a 220-n.mi. circular orbit, also inclined 28.5°, by using its orbital maneuvering system engines. Staging of the booster occurs 103 sec after launch at an altitude of 83 175 ft and a relative velocity of 2896 ft/sec.

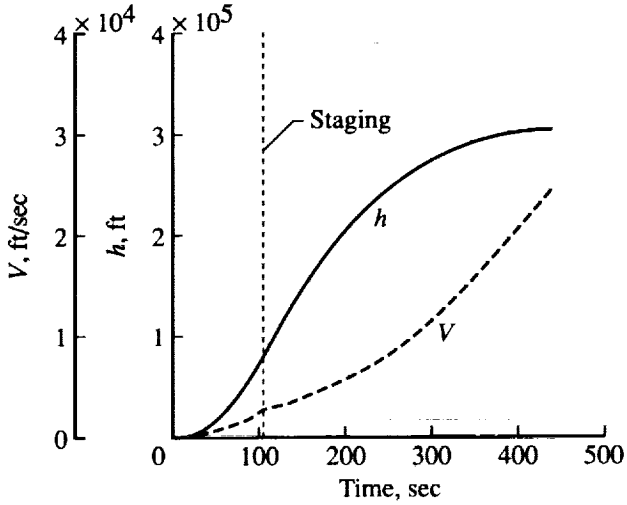

Figure 4. Velocity and altitude profiles during ascent.

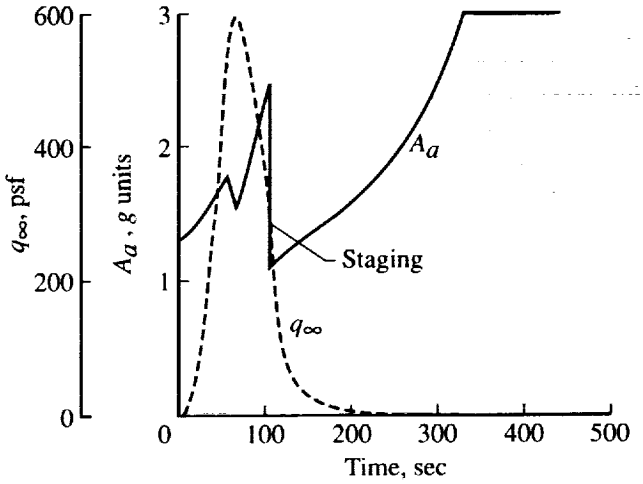

Figure 5. Dynamic pressure and axial acceleration during ascent.

Figure 5 shows that the axial acceleration limit of $3g$ is reached at 320 sec after launch. For the remainder of the ascent, the orbiter main engines are throttled to maintain a $3g$ axial acceleration. In order to meet the wing normal-force constraint, the launch vehicle flies a lofted ascent trajectory. Thus, the maximum dynamic pressure for the optimum constrained ascent trajectory is only 596 psf, which is well below the 800-psf limit. The dynamic pressure at staging is 308.6 psf.

The staging angle-of-attack constraint of $-1.7°$ was satisfied as shown in figure 6. During staging,

the pitch gimbal angle of the orbiter engine shifts from $-18°$ to $7°$. This large shift occurs because the booster propellants are nearly depleted just at staging and the booster engines are at full throttle. With throttling of the booster engines, the pitch gimbal angle shift of the orbiter engine can be reduced as detailed in reference 7.

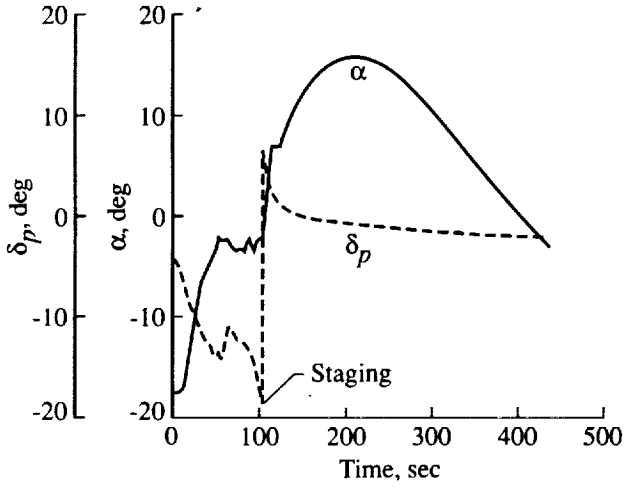

Figure 6. Pitch gimbal of engines and angle-of-attack profiles during ascent.

Analysis of Staging Maneuver

One of the significant design issues for any multistage vehicle is a safe separation at staging. The two-stage, fully reusable launch vehicle is different from any vehicle flown to date because both the orbiter and booster are winged. An additional complication is that because propellant is supplied to the orbiter from the booster during the boost phase, the booster (which is attached to the underside of the orbiter in a parallel stage configuration) has nearly depleted its propellants but the orbiter is fully loaded with propellant at staging. Also, the dynamic pressure at staging is approximately 10 times higher than the dynamic pressure at nominal staging of the Space Shuttle solid rocket boosters (SRB) from the external tank.

Assumptions

For this study, only the pitch plane (the XZ plane) of the staging maneuver was analyzed. The aerodynamic data base consisted of free-stream data for the individual orbiter and booster elements. Interference effects, which are caused by the close proximity of the two vehicles during the staging maneuver, were not included in the aerodynamic data base. In order to accurately assess interference aerodynamics at the nominal staging conditions, rigorous computational fluid dynamics techniques validated with wind tunnel tests would have to be employed, which is beyond the scope of the present study. The staging procedure developed in this study should be valid even though interference effects were not included in the aerodynamic data base.

The mass properties at staging for the booster and orbiter are shown in table 2. The orbiter is nearly 10 times heavier than the booster and has proportionately higher moments of inertia than the booster. For optimal payload performance, the launch vehicle is flown in a heads-up attitude during the ascent trajectory. Therefore, the booster is situated below the orbiter at staging.

Nominal trajectory conditions at staging initiation are shown in table 3, along with the nominal Space Shuttle SRB (STS-39) staging conditions for comparison. At staging, the launch vehicle is moving away from the launch site runway with a range of 10.5 n.mi. from the launch pad. Nominally, staging occurs at an altitude of 83 175 ft, a velocity of 2896 ft/sec, a dynamic pressure of 308.6 psf, and an angle of attack of $-1.7°$.

Table 2. Mass Properties at Staging

Property	Orbiter	Booster
Weight, lb	1 186 872	120 826
Total thrust, lb	1 395 200	0
X_{cg}, ft	98.78	87.36
Y_{cg}, ft	0	0
Z_{cg}, ft	0	−2.39
I_{xx}, slug-ft^2	3.955×10^6	0.444×10^6
I_{yy}, slug-ft^2	18.690×10^6	4.109×10^6
I_{zz}, slug-ft^2	20.092×10^6	4.262×10^6

Table 3. Nominal Conditions at Initiation of Staging Maneuver

Condition	Two-stage, fully reusable concept	Space Shuttle (STS-39)
Altitude, ft	83 175	156 441
V, ft/sec	2896	4094
γ, deg	34.9	32.6
α, deg	−1.7	1.2
Range to launch pad, n.mi.	10.5	25.4
q_∞, psf	308.6	22.7
Mach number	2.96	3.73
Time from lift-off, sec	104.8	125.3

Longitudinal Flight Control System of Booster

A longitudinal flight control system (fig. 7) was used to drive the booster elevons to control the angle of attack during the staging maneuver. This control system uses an angle-of-attack error signal coupled with pitch rate feedback to direct the booster. When the orbiter has been released from both booster attachment struts, the booster flight control system is given a commanded, or desired, angle of attack. The booster elevons are used to drive the booster to the commanded angle of attack and then maintain that angle of attack throughout the remainder of the staging maneuver. The commanded angle of attack chosen for this study was −10°. A more negative commanded angle of attack was not chosen because the booster cannot be trimmed at angles of attack below −15° at a Mach number of 3 with the present elevon control authority, and this choice leaves an angle-of-attack margin of 5°. A less negative commanded angle would not ensure that the booster would avoid recontact with the orbiter or avoid the orbiter engine plumes during the staging maneuver with sufficient margin.

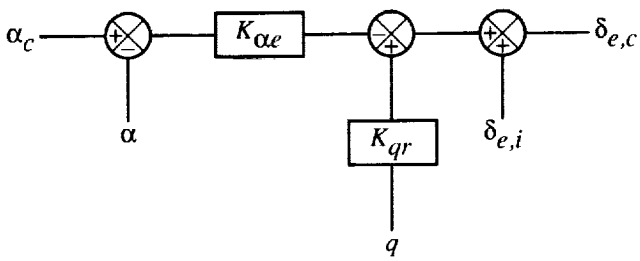

Figure 7. Longitudinal flight control system of booster for staging maneuver. $\delta_{e,i} = 0°$; $K_{\alpha e} = 1$; $K_{qr} = 2$ sec.

Staging Technique

The first simulation of staging was made at the nominal staging angle of attack of −1.7°, with the orbiter released simultaneously from both the forward and rearward attachment struts on the booster immediately after the booster engines were shut down. Figure 8 shows the movement of the booster relative to the orbiter for this case, in which the angle between the booster and orbiter (θ_R) was 0° at the instant that both the forward and rearward attachment struts were released. The longitudinal flight control system was not able to overcome the normal force and moment that caused the booster to pitch up and recontact the orbiter. The boundary of the orbiter engine plumes in figure 8 was estimated from photographs of the Space Shuttle at a Mach number of 3.5.

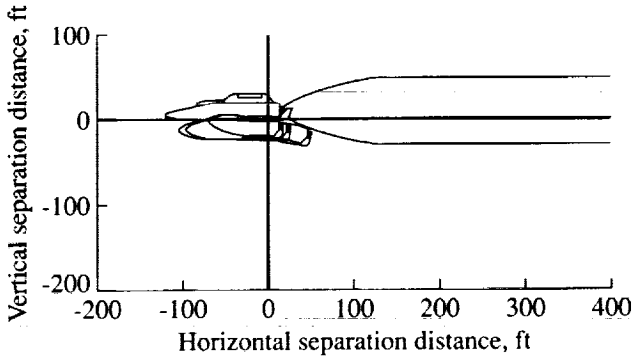

Figure 8. Separation with $\theta_R = 0°$. Booster shown at 0.5-sec intervals.

A new separation technique was developed to ensure that the booster would have the normal separation forces necessary to avoid recontact with the orbiter and to avoid the plumes from the orbiter engines. In this technique, the booster engines are shut down, the forward strut is immediately released, the booster rotates about the rearward struts, and the rearward struts are released when the angle between the booster and orbiter reaches 2°. Because of

Table 4. Nominal Conditions at Completion of Staging Maneuver

Condition	Booster	Orbiter
Altitude, ft	88 600	89 014
V, ft/sec	2732	2947
γ, deg	30	33.4
α, deg	−10	−4
Range to launch pad, n.mi.	11.8	11.8
Range to runway, n.mi.	15.8	15.8
q_∞, psf	204	241.9
Mach number	2.78	3
Time from lift-off, sec	108.2	108.2

the booster center-of-gravity location relative to the rearward struts, the aerodynamic forces cause the booster to rotate about the rearward struts. After the rearward struts are released, the booster is commanded to fly to an angle of attack of −10°. Figure 9 shows the elevon and angle-of-attack history for this maneuver starting at the instant that the orbiter is released from the rearward struts. Note that the initial angle of attack of the booster in figure 9 is −3.7° because the booster has rotated 2° with respect to the orbiter.

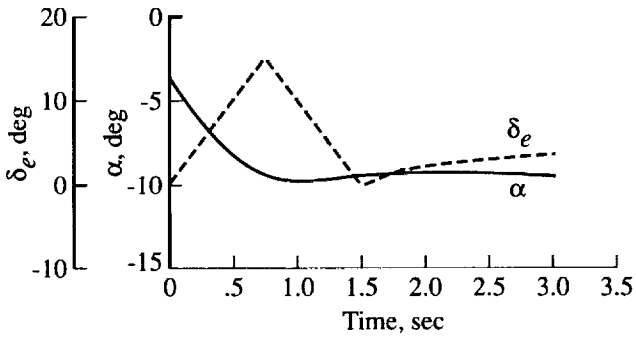

Figure 9. Elevon deflection and angle-of-attack profiles with $\theta_R = 2°$.

The elevons remain within their displacement limits throughout the staging maneuver and maintain the booster near the commanded angle of attack. Figure 10 shows the booster position, relative to the orbiter, for 3 sec after the orbiter has been released from the rear struts. After 3 sec, the booster is approximately 300 ft below and 300 ft behind the orbiter and is at a safe separation distance for the glideback maneuver to be initiated. Table 4 summarizes the booster and orbiter trajectory conditions at the completion of the staging maneuver.

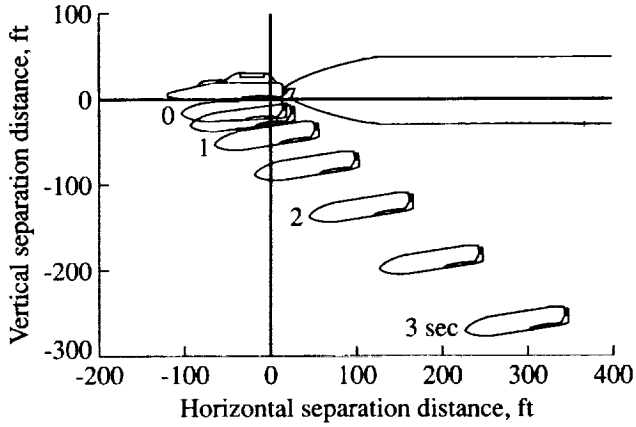

Figure 10. Separation with $\theta_R = 2°$. Booster shown at 0.5-sec intervals.

Range of Staging Angle of Attack

Using the new staging technique, separation trajectories were analyzed to determine the allowable range in staging angles of attack of the launch vehicle. Figure 11 summarizes the results of these separation trajectories by showing the rotational acceleration at the instant that the orbiter is released from the forward strut. The maximum staging angle of attack occurs at 2.6°, a position where the rotational acceleration is 0 and the booster will not rotate away from the orbiter. The minimum staging angle-of-attack limit occurs at the point where the booster longitudinal control system cannot keep the booster angle of attack from excessively overshooting −10° during the separation maneuver, beyond which the booster cannot be controlled with adequate margin.

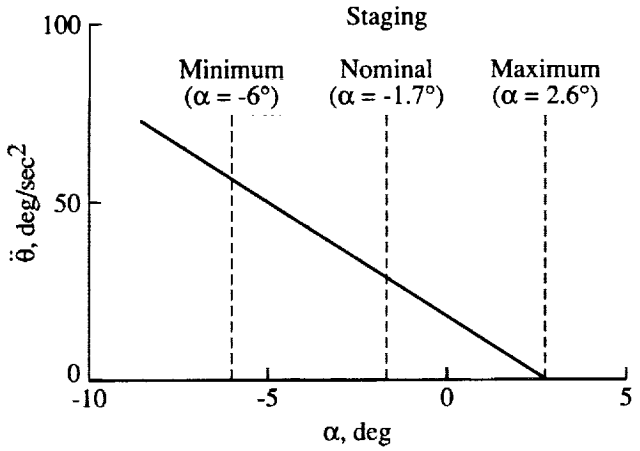

Figure 11. Rotational acceleration of booster about rear strut.

This minimum constraint occurs when the staging angle of attack is lower than $-6°$. As an example, figure 12 shows the elevon and angle-of-attack profiles for a staging angle of attack of $-7°$. The booster angle of attack is shown to overshoot the lower limit of $-10°$ during the staging maneuver and excessive elevon deflection angles are required. The staging angle of attack for the nominal ascent trajectory was chosen to be $-1.7°$, which is approximately the midpoint of the allowable 8.6° range in the staging angle of attack of the launch vehicle (fig. 11).

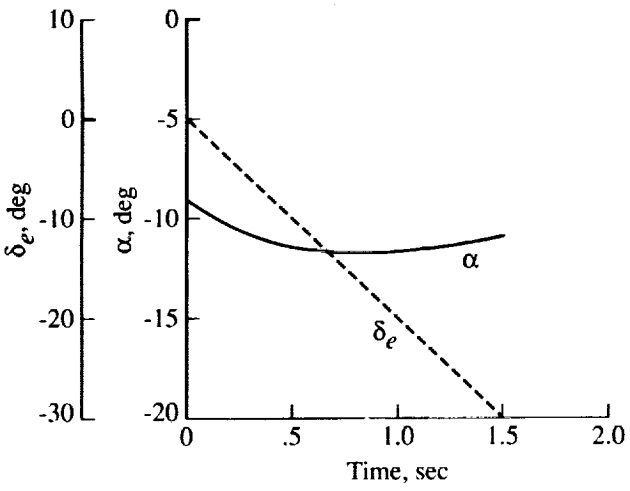

Figure 12. Elevon deflection and angle-of-attack profiles with $\theta_R = 2°$ and $\alpha_S = -7°$.

Analysis of Booster Glideback Guidance

For the booster glideback analysis, a guidance algorithm was developed, a nominal glideback trajectory was defined, and the guidance technique was tested with various atmospheric dispersions and other off-nominal conditions.

Development of Guidance Algorithm

The guidance algorithm developed for the booster glideback is divided into six phases which begin at the completion of the staging maneuver and end at touchdown on the runway (fig. 13). The overall strategy of the different phases includes the following: (1) arresting the booster downrange motion by turning back toward the launch area, (2) depleting the booster excess energy, (3) intersecting a heading alignment cylinder (HAC), (4) gliding on the HAC until lined up with the KSC Shuttle runway, (5) approaching the runway, and (6) performing a flare maneuver.

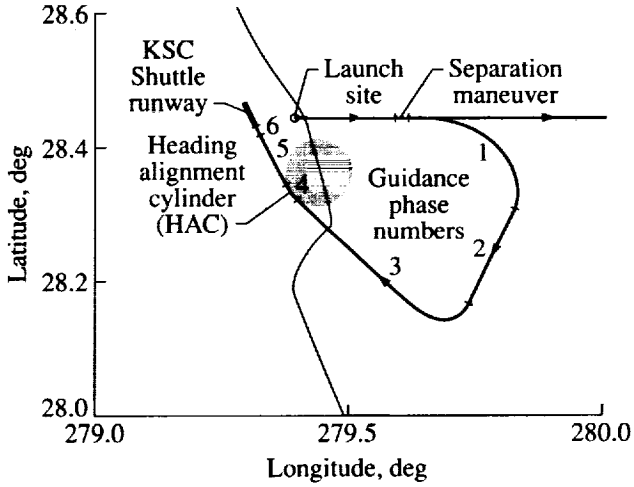

Figure 13. Phases of booster glideback guidance.

Phase 1—Initial turn after staging maneuver. Table 4 gives the trajectory conditions at the completion of the nominal staging maneuver. The first phase, which begins at the completion of staging, is the maneuver that arrests the downrange motion of the booster and turns it back toward the launch site runway. Before the turn begins, the booster has a heading angle of 90°; when the turn is completed, the booster has a heading angle of 210°. The heading angle of the runway is 330°.

The three-degrees-of-freedom POST program was used to find the optimum (minimum time) turning maneuver of phase 1 with the appropriate initial and final heading angles and a maximum normal acceleration of $2.3g$. Since the booster is designed for a maximum normal acceleration limit of $2.5g$, a margin of $0.2g$ was established to allow for possible increased loads from off-nominal conditions. An open-loop approximation to the optimum turning maneuver was modeled in which angle of attack was a function of Mach number and roll angle was a function of heading angle. A description of this maneuver follows.

For the first 20 sec of the turn, the booster angle of attack is calculated by using the expression

$$\alpha(t) = \alpha_i + \dot{\alpha}_i(t - t_i) \qquad (i = 0, 1)$$

where α_i is the initial angle of attack, $\dot{\alpha}$ is the time rate of change of angle of attack, t_i is the initial time, and t is the current time. The values of α_i and $\dot{\alpha}_i$, which were chosen in order to follow the angle-of-attack profile in the optimum turning maneuver, are shown in table 5. From 20 sec until the turn is completed, the angle of attack is a function of Mach number (fig. 14).

Table 5. Parameters in Guidance Angle-of-Attack Expression for Phase 1

t, sec	i	α_i, deg	$\dot{\alpha}$, deg/sec
$0 \leq t \leq 5$	0	−9.5	5.0
$5 < t \leq 20$	1	15.5	1.3

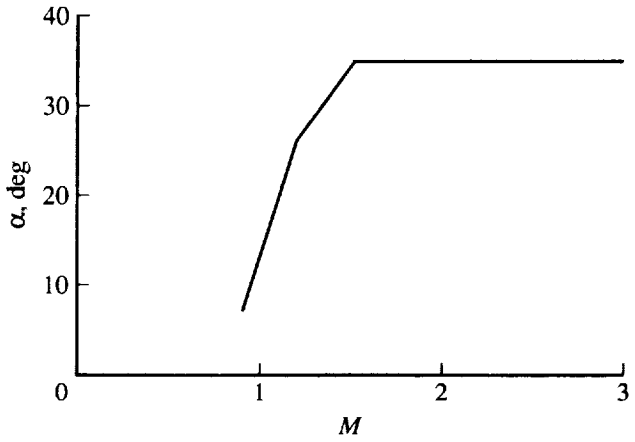

Figure 14. Booster angle-of-attack schedule for phases 1 and 2.

For the first 10 sec of the turn, the booster roll angle is calculated by using the expression

$$\phi(t) = \phi_i + \dot{\phi}_i(t - t_i) \qquad (i = 0, 1)$$

where ϕ_i is the initial roll angle and $\dot{\phi}_i$ is the time rate of change of roll angle. The values of ϕ_i and $\dot{\phi}_i$, which were chosen in order to follow the roll-angle profile in the optimum turning maneuver, are shown in table 6. From 10 sec until the turn is completed, the roll angle is a function of heading angle (fig. 15).

Phase 2—Excess performance dissipation. When the booster reaches a heading angle of 210°, phase 2 begins and the booster is rolled to 0° at a rate of 20 deg/sec. The roll angle is then modulated by feedback to keep the booster on a 210° heading angle while the excess performance is dissipated. The angle of attack continues to follow the Mach number schedule used in phase 1 (fig. 14) until an angle of attack of 6.5° is reached. For the remaining portion of phase 2, the angle of attack is kept at 6.5°.

Table 6. Parameters in Guidance Roll-Angle Expression for Phase 1

t, sec	i	ϕ_i, deg	$\dot{\phi}$, deg/sec
$0 \leq t \leq 5$	0	0	13.3
$5 < t \leq 10$	1	66.5	10.7

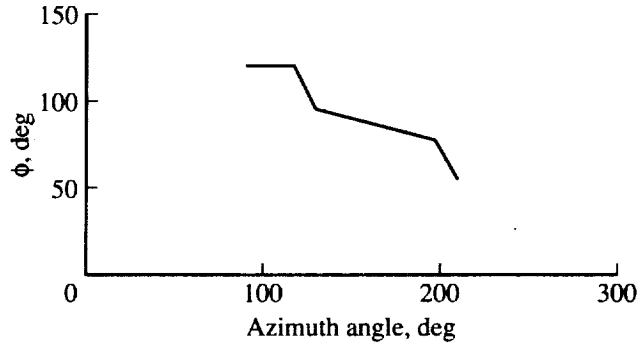

Figure 15. Booster roll-angle schedule for phase 1.

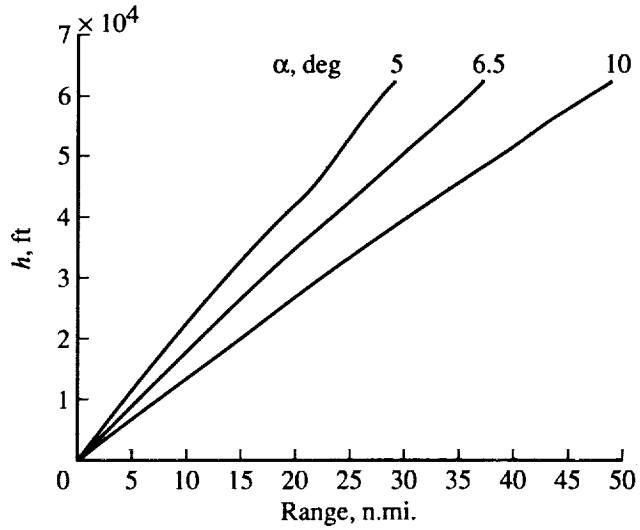

Figure 16. Potential range of booster.

The purpose of phase 2 is to deplete the booster excess performance. The guidance algorithm continuously calculates the range from the booster current

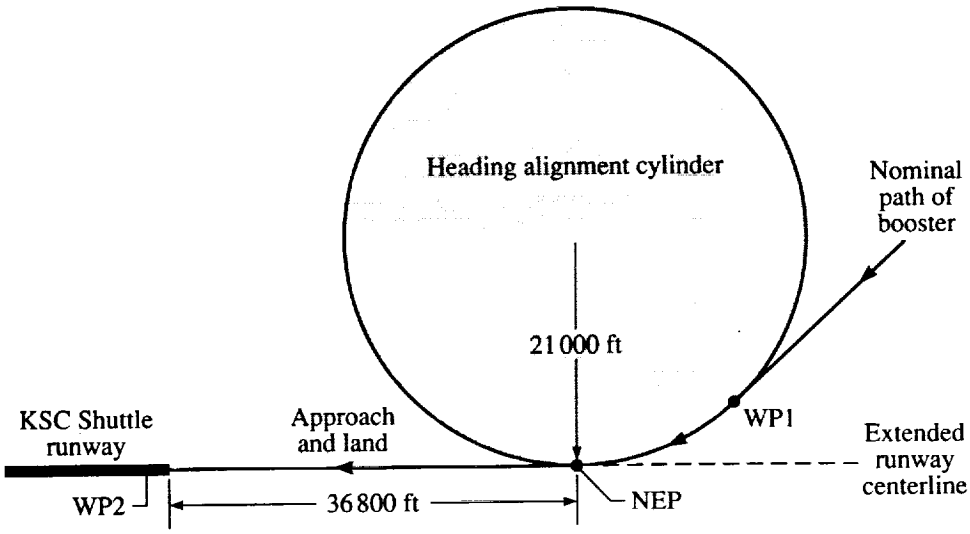

Figure 17. Geometry of heading alignment cylinder.

position to the target point on the runway. The guidance algorithm also calculates the booster potential range at its current altitude and angle of attack using the plot found in figure 16. Once the booster potential range to the runway converges to the actual range to the runway, the third guidance phase is initiated.

Phase 3—Acquisition of heading alignment cylinder. Phase 3 consists of the turn and glide to the heading alignment cylinder (HAC). Throughout phase 3, the angle of attack is modulated by feedback about the nominal angle of attack of 6.5° to keep the booster potential range equal to the actual range to the runway. The booster has approximately equal range margins above and below its potential range at an angle of attack of 6.5°. The upper performance limit is defined by the booster maximum L/D, which occurs at an angle of attack of 10°. The lower performance limit was set at 5°. Figure 16 shows the booster altitude-dependent potential range for angles of attack between 5° and 10°.

During phase 3, the booster roll angle is modulated to keep the booster headed toward way point 1 (WP1), which is the target point on the HAC (fig. 17). This HAC concept, which is similar to the one used by the Shuttle orbiter, consists of an imaginary cylinder that is tangent to the extension of the runway centerline. The point where the HAC and the extension of the runway centerline intersect is called the nominal entry point (NEP). For the guidance algorithm for the booster glideback, the HAC is defined with a radius of 21 000 ft and a distance to the runway threshold of 36 800 ft. The radius was chosen so that the roll angle of the booster, while on the HAC, would be in the range from 10° to 20°. The distance to the runway threshold was dictated by the desired flight-path angle during the approach phase.

Phase 4—Heading alignment cylinder. Phase 4 guidance begins when the booster reaches WP1. The booster roll angle is modulated by feedback to maintain a constant radius turn equal to the radius of the HAC. For simplicity, the angle of attack throughout phase 4 is maintained at the final angle of attack of phase 3. When the booster has traveled around the cylinder to the point where it is aligned with the runway centerline (i.e., NEP), phase 5 is initiated and the booster rolls to 0°.

Phase 5—Approach. Phase 5 begins when the booster is at the NEP and ends when the booster reaches an altitude of 1000 ft. For phase 5, a reference aim point was defined to be 40 ft down the runway, which is 2210 ft short of the desired touchdown position used in phase 6. The instantaneous flight-path angle necessary for the booster to fly toward the reference aim point was defined as γ_{ref}. The commanded booster angle of attack during phase 5 was calculated using the expression

$$\alpha_c = \alpha_i + K_{\alpha d5}\,(\gamma_{\text{ref}} - \gamma) + K_{\alpha r5}\,(d\gamma/dt)$$

where α_i is the initial angle of attack of phase 5, the displacement ($K_{\alpha d5}$) and rate gains ($K_{\alpha r5}$) are 3 and 0.153 sec, respectively, and γ and $d\gamma/dt$ are the current flight-path angle and flight-path-angle rate, respectively. The values of the gains were chosen to minimize the integrated error between the actual γ and γ_{ref}. If the initial flight-path angle of phase 5 did not agree with the initial reference flight-path angle,

the error was reduced linearly over the first 20 sec of phase 5.

The roll angle was modulated to maintain the alignment of the booster with the runway centerline. If the booster deviated from the extension of the centerline, the expression used to calculate the commanded roll angle to return to the centerline was

$$\phi_c = -K_{\phi d5} Y_{rt} - K_{\phi r5} \dot{Y}_{rt}$$

where the displacement ($K_{\phi d5}$) and rate gains ($K_{\phi r5}$) are 0.1 deg/ft and 0.2 deg-sec/ft, respectively, Y_{rt} is the distance from the booster to the extension of the centerline, and $\dot{Y}_{rt}$ is the velocity component perpendicular to the extension of the centerline. The values of these gains were chosen based on previous experience.

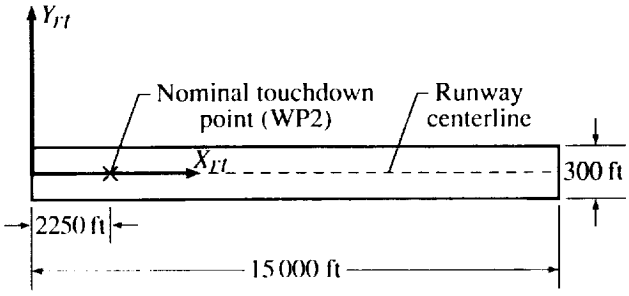

Figure 18. Coordinate system of KSC Shuttle runway.

Phase 6—Flare and touchdown. At an altitude of 1000 ft the booster enters phase 6, which is the flare maneuver and touchdown on the runway. As with the Shuttle, the desired touchdown point is approximately 15 percent of the length down the runway (fig. 18). A technique was developed that ensured that the booster would touch down near the target point (way point 2 (WP2)) even when encountering extreme off-nominal conditions. A nominal flare maneuver was developed in which the booster had a descent rate of -1.4 ft/sec at touchdown on the nominal target point. From this nominal trajectory, a relationship between flight-path angle and altitude was developed based on a curve fit of the nominal γ profile

$$\gamma_{\text{ref}} = \gamma_0 + \gamma_1 h + \gamma_2 h^2 + \gamma_3 h^3$$

where γ_{ref} is the desired flight-path angle at altitude h. Differentiating this expression gives

$$d\gamma_{\text{ref}}/dh = \gamma_1 + 2\gamma_2 h + 3\gamma_3 h^2$$

where $d\gamma_{\text{ref}}/dh$ is the desired flight-path-angle rate at altitude h. The flight-path-angle rate must be transformed from $d\gamma_{\text{ref}}/dh$ to $d\gamma_{\text{ref}}/dt$ using the chain rule given as

$$d\gamma_{\text{ref}}/dt = (d\gamma_{\text{ref}}/dh)(dh/dt)$$

where dh/dt is the altitude rate. To calculate the commanded angle of attack of the booster, the relationship used was

$$\alpha_c = \alpha_i + K_{\alpha d6}(\gamma_{\text{ref}} - \gamma) + K_{\alpha r6}\left[(d\gamma_{\text{ref}}/dt) - (d\gamma/dt)\right]$$

where the displacement ($K_{\alpha d6}$) and rate gains ($K_{\alpha r6}$) are 12 and 1.0 sec, respectively, and γ and $d\gamma/dt$ are the current flight-path angle and flight-path-angle rate, respectively. The values of these gains were also chosen based on previous experience.

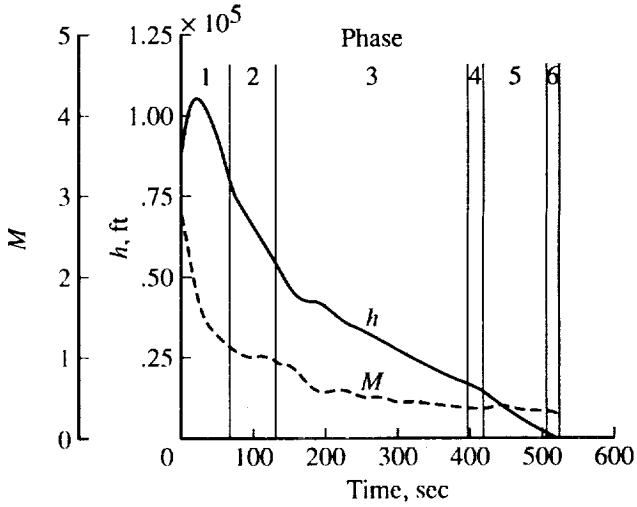

Figure 19. Profiles of Mach number and altitude for nominal booster glideback trajectory.

Nominal Glideback Trajectory

For the development of the nominal glideback trajectory, the 1976 U.S. Standard Atmosphere (ref. 12) was used. Figures 19–22 show the nominal glideback trajectory from the completion of the staging maneuver to touchdown on the runway using the guidance algorithm described in the previous section entitled "Development of Guidance Algorithm." The booster requires 523 sec to complete the nominal glideback trajectory. The phase 1 turn is completed during the first 70 sec. The booster remains in phase 2 for 50 sec while its excess energy is being dissipated. At 120 sec into the glideback, the booster initiates the HAC acquisition phase and reaches the HAC at 395 sec. At 415 sec the booster comes off the HAC and is aligned with the runway. The flare maneuver starts at 510 sec with touchdown occurring at 523 sec. The nominal

touchdown position is on the centerline, at 2250 ft down the 15 000-ft runway, with a descent rate of 1.4 ft/sec. Figure 18 shows the nominal touchdown position in the runway coordinate system.

Figure 19 shows the Mach number and altitude profiles for the nominal glideback trajectory. The rapid deceleration of the booster after staging is evident in the Mach number profile. During the first 100 sec, the booster decelerates from a Mach number of 2.8 to below 1.0. The booster remains at subsonic speeds for the remainder of the glideback. The booster reaches a maximum altitude of 110 000 ft at 20 sec into the glideback. At 200 sec into the glideback, the booster enters into an equilibrium glide until the HAC is reached at 395 sec.

The roll-angle and angle-of-attack profiles are shown in figure 20. The angle of attack reaches a maximum of 35°, and the roll angle reaches a maximum of 120° during the phase 1 turn. The roll-angle profile shows when the phase 1 turn is completed (70 sec), when the booster turns toward the HAC (120 sec), and when the booster is on the HAC (395–410 sec). The angle-of-attack profile shows that throughout phases 2–4 the booster flies near the desired angle of attack of 6.5°.

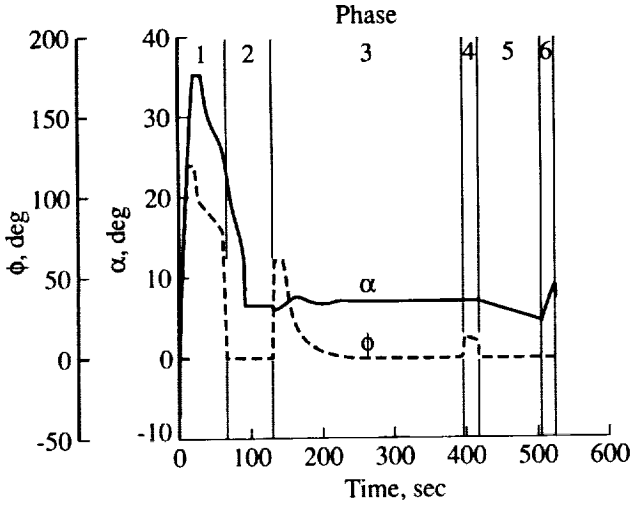

Figure 20. Profiles of roll angle and angle of attack for nominal booster glideback trajectory.

Figure 21 shows the flight-path angle and normal acceleration profiles. The maximum normal acceleration during the nominal glideback is 2.3g, which is below the 2.5g limit. The flight-path-angle profile shows that during the glideback, the flight-path angle varies from a maximum of 30°, at staging completion to a minimum of −45° just after the maximum altitude is attained.

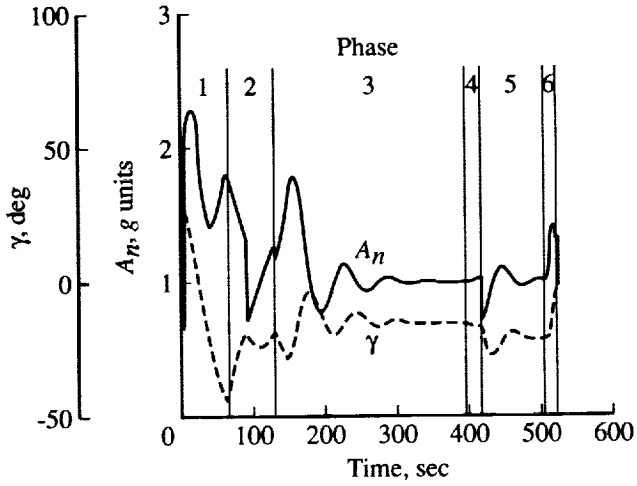

Figure 21. Profiles of flight-path angle and normal acceleration for nominal booster glideback trajectory.

The elevon deflection angle and range profiles are shown in figure 22. The elevon deflection angle remains within the limits of −30° and 20° throughout the glideback. The booster reaches a maximum range of 28 n.mi. from the runway.

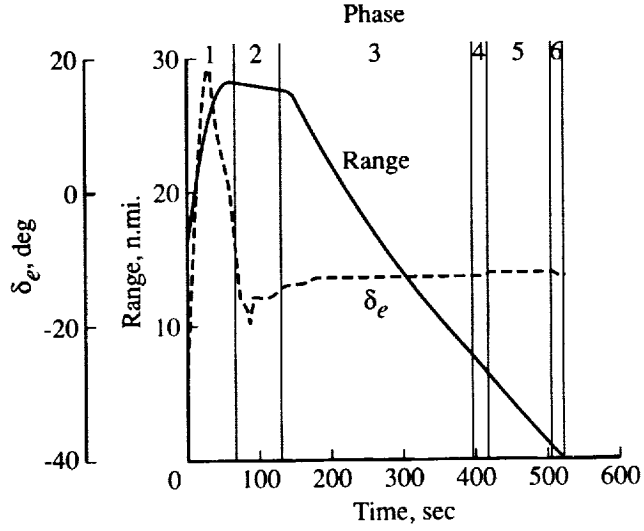

Figure 22. Profiles of elevon deflection angle and range for nominal booster glideback trajectory.

Off-Nominal Glideback Trajectories

Atmospheric dispersions. The initial off-nominal conditions used in the guidance sensitivity analysis were constant bias factors applied to the 1976 U.S. Standard Atmospheric density which was multiplied by factors of 0.9 and 1.1. Table 7 shows the booster touchdown conditions with the high- and low-density profiles along with the nominal booster

Table 7. Booster Touchdown Conditions With Variations in 1976 U.S. Standard Atmospheric Density Profiles

Condition	X_{rt}, ft	$\dot{X}_{rt}$, ft/sec	Y_{rt}, ft	$\dot{Y}_{rt}$, ft/sec	$\dot{h}$, ft/sec
Nominal	2250	305	0	0	−1.4
$1.1 \times \rho_{76}$	2256	284	0	0	−1.3
$0.9 \times \rho_{76}$	2247	326	0	0	−1.3

Table 8. Booster Touchdown Conditions With Constant Head, Tail, and Cross Winds

Condition	X_{rt}, ft	$\dot{X}_{rt}$, ft/sec	Y_{rt}, ft	$\dot{Y}_{rt}$, ft/sec	$\dot{h}$, ft/sec
Nominal	2250	305	0	0	−1.4
Head	2140	226	0	0	−1.4
Tail	2091	379	0	0	−1.4
Left cross	2239	299	11.7	3.2	−1.4
Right cross	2256	303	−11.4	−3.4	−1.5

touchdown conditions. (See fig. 18 for runway coordinate system definition.) In both cases the booster landed within 6 ft of the nominal target point and had a lower touchdown velocity (284 ft/sec) for the high-density atmosphere and a higher touchdown velocity (326 ft/sec) for the low-density atmosphere.

Glideback trajectories were modeled with constant head, tail, and cross winds incorporated. The wind speed was assumed to be 22 knots, which was consistent with the maximum magnitude that was used in the Shuttle orbiter guidance evaluations. Table 8 shows the booster touchdown conditions for these four glideback cases. The constant head and tail winds had a significant effect on the X-component of the touchdown velocity, and the constant cross winds had a significant effect on the Y-component of the touchdown velocity. However, all four booster simulations ended with a successful runway landing. The side velocity at touchdown for the two cross wind cases (3.2 ft/sec and −3.4 ft/sec) resulted in a sideslip angle range from approximately $-1°$ to $1°$, which was well below the sideslip angle range from $-3°$ to $3°$ that the landing gear was designed to handle.

To simulate more realistic atmospheric conditions, mean density profiles and wind profiles for each month of the year at the launch site were determined by using the GRAM model. In addition, 10 perturbed and $\pm 3\sigma$ perturbed atmospheres were determined for a single month of the year. July was chosen for these perturbed atmospheres. Figures 23–25 show a composite of all the atmospheres that were generated with the GRAM for use in this study. In figure 23, the GRAM atmospheric densities are divided by the 1976 U.S. Standard Atmospheric density to simplify the comparisons. Over the altitude range that the booster covers during the glideback, the GRAM densities range from 6 percent lower to over 18 percent higher than the 1976 U.S. Standard Atmospheric density. The east-west component of the winds (fig. 24) for the GRAM atmospheres varies from 100 ft/sec east to 125 ft/sec west. The maximum north-south component of the winds (fig. 25) is much smaller and is less than 20 ft/sec.

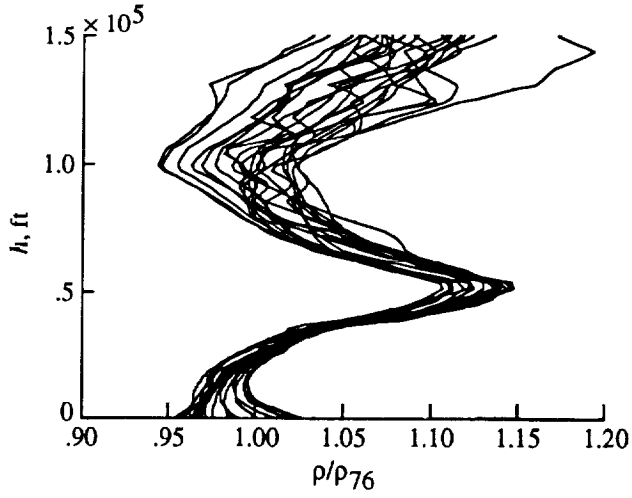

Figure 23. Variation of monthly and perturbed atmospheric densities.

Table 9. Booster Touchdown Conditions With GRAM Atmospheric Density Variations for Monthly Mean Density With No Wind

Condition	X_{rt}, ft	$\dot{X}_{rt}$, ft/sec	Y_{rt}, ft	$\dot{Y}_{rt}$, ft/sec	$\dot{h}$, ft/sec
Nominal	2250	305	0	0	−1.4
January	2247	305			−1.4
February	2238	305			−1.4
March	2236	307			−1.3
April	2242	309			−1.2
May	2228	311			−1.4
June	2241	313			−1.4
July	2230	314			−1.5
August	2232	314			−1.4
September	2263	313			−1.3
October	2241	311			−1.4
November	2272	307			−1.2
December	2247	306			−1.3

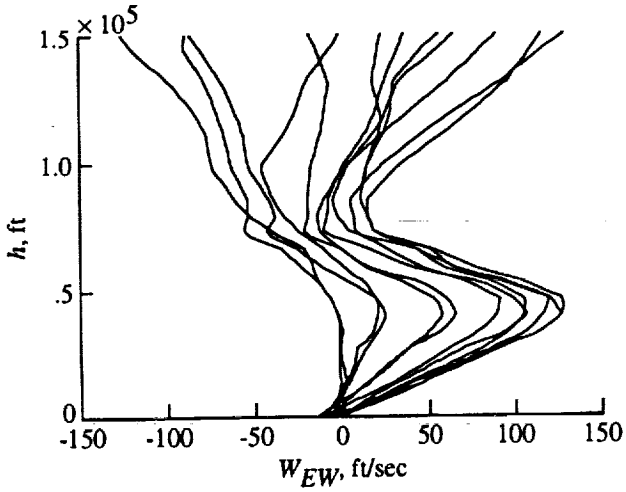

Figure 24. Variation of monthly east-west wind components.

Tables 9 and 10 show the booster touchdown conditions with the monthly mean densities without and with winds, respectively. Results of the glideback trajectories for 10 perturbed July atmospheres as well as $\pm 3\sigma$ variations of the July atmosphere are shown in table 11. The landing conditions for all these trajectories are close to the nominal landing conditions. Also, none of the vehicle constraints are violated throughout any of these trajectories.

Aerodynamic dispersions. Errors in the predicted booster aerodynamics were simulated by multiplying the lift and drag coefficients of the booster by factors of 0.9 and 1.1. The results of these trajectories are shown in table 12. In the high-drag case and low-lift case, the booster lands closer to the beginning of the runway than any of the other off-nominal cases. The descent rate at touchdown for these two cases is higher than the other off-nominal cases, but it is still well within the descent rate limit of 3 ft/sec. None of the aerodynamic dispersion cases violate the vehicle constraints. Also, the landing conditions are again very close to the nominal conditions.

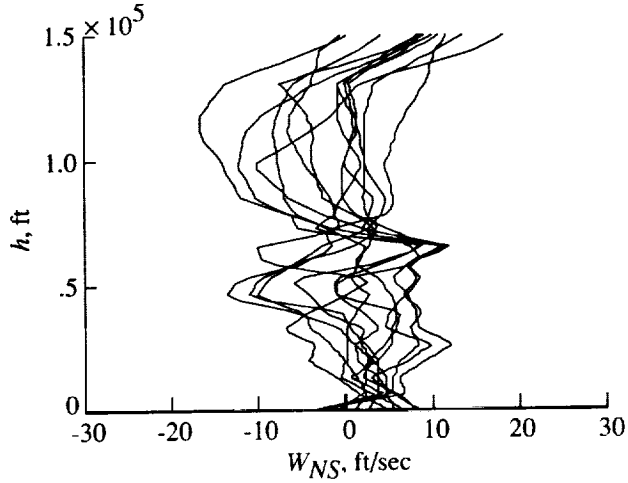

Figure 25. Variation of monthly north-south wind components.

Staging state dispersions. The errors in the staging conditions were simulated by adding and subtracting 10 percent to the nominal staging altitude, velocity, and flight-path angle. Table 13 summarizes the results for these glideback trajectories. The guidance algorithm was able to adjust to these errors in

Table 10. Booster Touchdown Conditions With GRAM Atmospheric Density Variations for Monthly Mean Density With Wind

Condition	X_{rt}, ft	$\dot{X}_{rt}$, ft/sec	Y_{rt}, ft	$\dot{Y}_{rt}$, ft/sec	$\dot{h}$, ft/sec
Nominal	2250	305	0	0	−1.4
January	2134	273	−1.8	−.5	−1.4
February	2123	268	−1.2	−.3	−1.4
March	2108	273	−.3	−.1	−1.3
April	2156	288	.4	.1	−1.2
May	2250	308	−.4	−.1	−1.4
June	2241	323	−.6	−.3	−1.4
July	2235	326	.2	0	−1.5
August	2242	324	−.4	−.2	−1.4
September	2254	321	−2.4	−.8	−1.3
October	2234	309	−3.8	−1.1	−1.4
November	2197	291	−3.8	−1.0	−1.2
December	2149	278	−2.6	−.7	−1.3

Table 11. Booster Touchdown Conditions With GRAM Atmospheric Density Variations for Perturbations for July With Wind

Condition	X_{rt}, ft	$\dot{X}_{rt}$, ft/sec	Y_{rt}, ft	$\dot{Y}_{rt}$, ft/sec	$\dot{h}$, ft/sec
Perturbation					
1	2206	329	0.2	0	−1.3
2	2243	330	↓	↓	−1.2
3	2245	328	↓	↓	−1.5
4	2224	330	↓	↓	−1.4
5	2246	330	.3	↓	−1.4
6	2232	329	.2	↓	−1.3
7	2211	331	↓	↓	−1.2
8	2213	330	↓	↓	−1.3
9	2235	329	↓	↓	−1.3
10	2212	331	.3	↓	−1.5
Perturbation variation					
3σ	2229	321	0.3	0	−1.5
-3σ	2223	331	1	0	−1.5

Table 12. Booster Touchdown Conditions With Constant Variations in Predicted Aerodynamics

Condition	X_{rt}, ft	$\dot{X}_{rt}$, ft/sec	Y_{rt}, ft	$\dot{Y}_{rt}$, ft/sec	$\dot{h}$, ft/sec
Nominal	2250	305	0	0	−1.4
Drag:					
$1.1 \times C_{D,\text{nom}}$	2036	259	0	0	−1.7
$0.9 \times C_{D,\text{nom}}$	2186	364	0	0	−1.0
Lift:					
$1.1 \times C_{L,\text{nom}}$	2219	335	0	0	−1.4
$0.9 \times C_{L,\text{nom}}$	1931	263	0	0	−1.7

Table 13. Booster Touchdown Conditions With Variations in Predicted Staging Parameters

Condition	X_{rt}, ft	$\dot{X}_{rt}$, ft/sec	Y_{rt}, ft	$\dot{Y}_{rt}$, ft/sec	$\dot{h}$, ft/sec
Nominal	2250	305	0	0	−1.4
Staging altitude:					
10 percent high	2239	303	0	0	−1.4
10 percent low	2247	303	0	0	−1.4
Staging velocity:					
10 percent high	2245	302	0	0	−1.4
10 percent low	2246	306	0	0	−1.4
Staging flight-path angle:					
10 percent high	2233	305	0	0	−1.4
10 percent low	2252	306	0	0	−1.4

Table 14. Range of Touchdown Conditions for Glideback Simulations

Condition	Minimum	Nominal	Maximum
Total glideback time, sec	483	525	651
X, ft	1931	2250	2272
$\dot{X}$, ft/sec	226	305	379
Y, ft	−11.4	0	11.6
$\dot{Y}_{rt}$, ft/sec	−3.4	0	3.2
$\dot{h}$, ft/sec	−1.0	−1.4	−1.7

staging conditions and land the booster close to the nominal position and velocity while remaining within the vehicle constraints, except for the case in which the staging altitude was 10 percent low. For this case, the normal acceleration reached a maximum of 2.75g during the phase 1 turning maneuver. Further analysis showed that if the lowest staging altitude is limited to 6 percent below the nominal staging altitude, the normal acceleration limit is not violated.

Summary of off-nominal glideback trajectories. Table 14 shows the range of touchdown conditions for all the off-nominal cases. The time at touchdown varied widely from 483 to 651 sec. The booster touchdown position varied from 1931 to 2272 ft down the runway and was within 12 ft of the runway centerline. The velocity at touchdown varied from 226 ft/sec to 379 ft/sec with the side velocity less than 3.5 ft/sec. All the off-nominal cases had a descent rate at touchdown below 1.7 ft/sec.

All the trajectories discussed in this section are plotted together in figures 26–31. Figure 26 shows the wide range of paths that the booster followed to reach the HAC, and figure 27 shows the corresponding altitude profiles. The normal acceleration profiles (fig. 28) show that all but one off-nominal case remained below the 2.5g normal acceleration constraint during the early part of the glideback. This

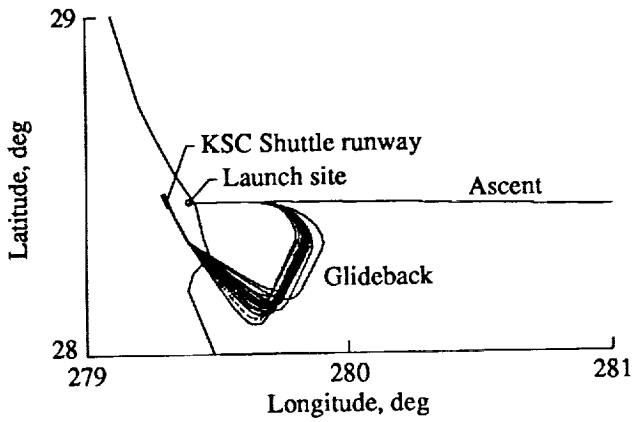

Figure 26. Ground track profiles of off-nominal glideback trajectories of booster.

particular case, the low initial altitude case, was discussed in the previous subsection entitled "Staging state dispersions." Two simulations have flare maneuvers with a normal acceleration above 2.5g. Further refinement of the guidance algorithm would reduce the normal acceleration for these two cases below the maximum constraint. The angle-of-attack histories (fig. 29) vary significantly depending on the off-nominal conditions but never reach the upper and lower limits of 10° and 5° during phases 2–5. The individual roll-angle histories (fig. 30) are similar but show that the phases are occurring at widely varying times. The elevon deflections (fig. 31) remained within the limits of −30° and 20° during all the off-nominal glideback trajectories.

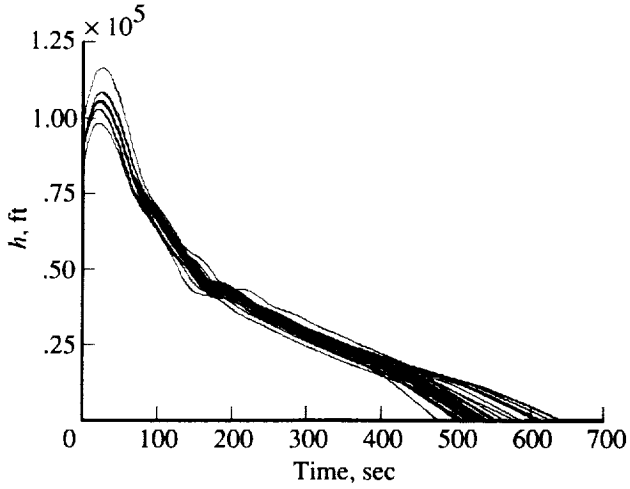

Figure 27. Altitude profiles of off-nominal glideback trajectories of booster.

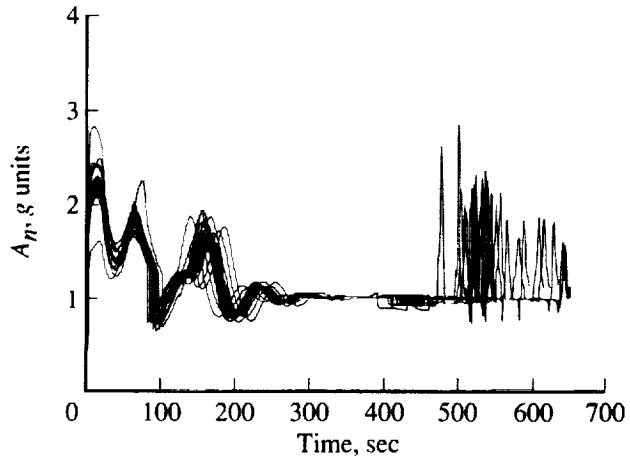

Figure 28. Normal acceleration profiles of off-nominal glideback trajectories of booster.

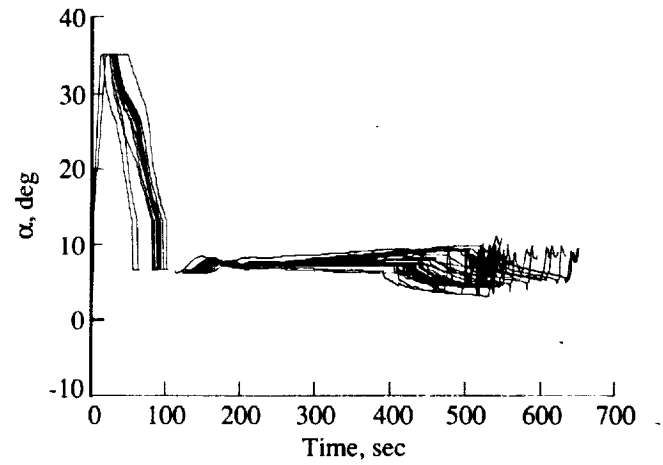

Figure 29. Angle-of-attack profiles of off-nominal glideback trajectories of booster.

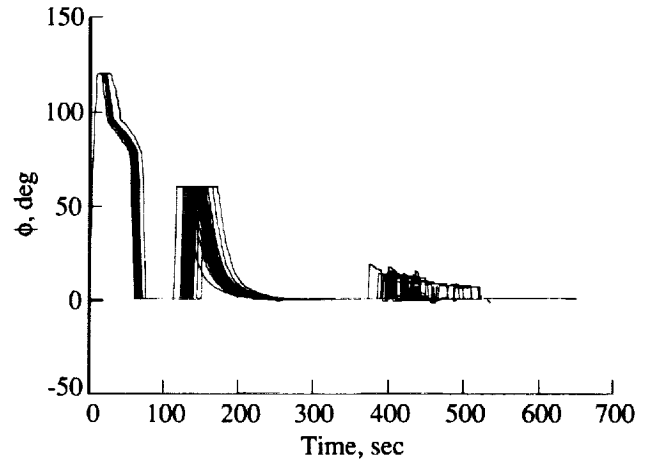

Figure 30. Roll-angle profiles of off-nominal glideback trajectories of booster.

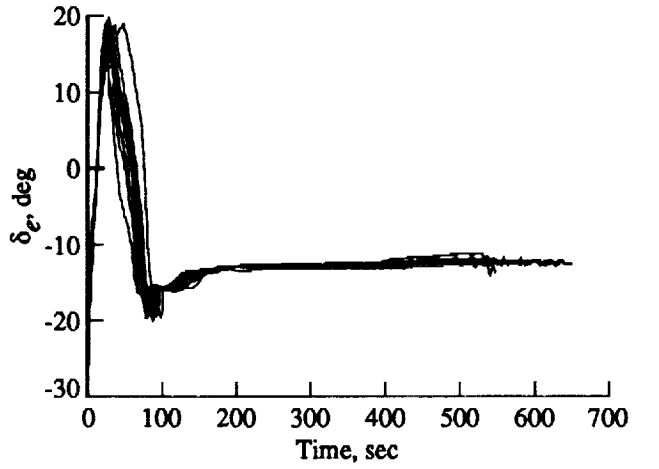

Figure 31. Elevon deflection profiles of off-nominal glideback trajectories of booster.

Concluding Remarks

Many concepts have been studied that represent a follow-on to the current Shuttle launch system. One of these concepts is a two-stage, fully reusable, winged, vertical-takeoff launch vehicle that utilizes a glideback booster. Two major design issues for this class of vehicle, the staging maneuver and the booster glideback guidance, have been analyzed. These analyses have shown that the staging maneuver is controllable and the booster glideback maneuver has adequate margin to adjust to off-nominal conditions.

A staging technique was developed that ensured a safe separation of the booster from the orbiter while avoiding recontact with the orbiter and interference from the exhaust plumes of the orbiter engines. The booster could be controlled aerodynamically during the staging maneuver, and therefore a reaction control system was not required. Separation trajectories were modeled with various angles of attack at staging initiation to determine the allowable range in staging angle of attack. The nominal staging angle of attack ($-1.7°$) was chosen to be in the middle of the $8.6°$ allowable range in staging angle of attack.

A guidance algorithm for the booster glideback to the launch site was developed, and this algorithm was incorporated into a three-degrees-of-freedom trajectory program with longitudinal trim so that elevon deflections required for trim could be calculated. Glideback simulations were modeled with a variety of off-nominal atmospheric, staging, and booster aerodynamic conditions with the booster landing with a descent rate less than 1.7 ft/sec within a 320-ft range of the target touchdown point.

NASA Langley Research Center
Hampton, VA 23681-0001
March 12, 1993

References

1. Freeman, Delma C., Jr.: The New Space Transportation Begins Today. *Astronaut. & Aeronaut.*, vol. 21, no. 6, June 1983, pp. 36–37, 48.

2. Martin, James A.: Orbit on Demand: In This Century If Pushed. *Aerosp. America*, vol. 23, no. 2, Feb. 1985, pp. 46–48.

3. Talay, Theodore A.: Shuttle II Progress Report. Paper presented at the Twenty-Fourth Space Congress Proceedings (Cocoa Beach, Florida), Apr. 21–24, 1987.

4. Talay, Theodore A.; and Morris, W. Douglas: Advanced Manned Launch Systems. Paper presented at AAAF, DGLR, Royal Aeronautical Society, and ESA Second European Aerospace Conference on Progress in Space Transportation (Bonn, Federal Republic of Germany), May 22–24, 1989.

5. Naftel, J. C.; and Powell, R. W.: Flight Analysis for a Two-Stage Launch Vehicle With a Glideback Booster. *J. Guid., Control, & Dyn.*, vol. 8, no. 3, May–June 1985, pp. 340–343.

6. Freeman, Delma C., Jr.; and Fournier, Roger H.: *Static Aerodynamic Characteristics of a Winged Single-Stage-to-Orbit Vehicle at Mach Numbers From 0.3 to 4.63.* NASA TP-1233, 1978.

7. Hurley, M. J.: *Digital Program P5255—A Six-Degree, Multiple-Body Separation Simulation for Hinged and/or Linked Lifting-Entry Vehicles. Volume I—Equation/ Program Development.* GDC-ERR-1377, General Dynamics, Convair Div., Dec. 1969.

8. Brauer, G. L.; Cornick, D. E.; and Stevenson, R.: *Capabilities and Applications of the Program To Optimize Simulated Trajectories (POST)—Program Summary Document.* NASA CR-2770, 1977.

9. Justus, C. G.; Fletcher, G. R.; Gramling, F. E.; and Pace, W. B.: *The NASA/MSFC Global Reference Atmospheric Model—MOD 3 (With Spherical Harmonic Wind Model).* NASA CR-3256, 1980.

10. Justus, C. G.; Alyea, F. N.; Cunnold, D. M.; Blocker, R. S.; and Johnson, D. L.: *GRAM-88—Improvements in the Perturbation Simulations of the Global Reference Atmospheric Model.* ESS44-11-9-88, NASA Marshall Space Flight Center, Nov. 1988.

11. Powell, Richard W.; Naftel, J. Christopher; and Cruz, Christopher I.: Flight Control Issues of the Next Generation Space Transportation Launch Vehicles. Paper presented at the 75th Symposium of the Flight Mechanics Panel on Space Vehicle Flight Mechanics (Luxembourg), Nov. 13–16, 1989.

12. *U.S. Standard Atmosphere, 1976.* National Oceanic and Atmospheric Adm., National Aeronautics and Space Adm., and United States Air Force, Oct. 1976.

REPORT DOCUMENTATION PAGE

Form Approved
OMB No. 0704-0188

1. AGENCY USE ONLY *(Leave blank)*

2. REPORT DATE
April 1993

3. REPORT TYPE AND DATES COVERED
Technical Paper

4. TITLE AND SUBTITLE
Analysis of the Staging Maneuver and Booster Glideback Guidance for a Two-Stage, Winged, Fully Reusable Launch Vehicle

5. FUNDING NUMBERS
WU 906-11-01-01

6. AUTHOR(S)
J. Christopher Naftel and Richard W. Powell

7. PERFORMING ORGANIZATION NAME(S) AND ADDRESS(ES)
NASA Langley Research Center
Hampton, VA 23681-0001

8. PERFORMING ORGANIZATION REPORT NUMBER
L-17066

9. SPONSORING/MONITORING AGENCY NAME(S) AND ADDRESS(ES)
National Aeronautics and Space Administration
Washington, DC 20546-0001

10. SPONSORING/MONITORING AGENCY REPORT NUMBER
NASA TP-3335

11. SUPPLEMENTARY NOTES
Based on thesis submitted by Naftel in partial fulfillment of the requirements for the Degree of Master of Science, George Washington University, Washington, DC; the advisor was Powell.

12a. DISTRIBUTION/AVAILABILITY STATEMENT
Unclassified–Unlimited

Subject Category 15

12b. DISTRIBUTION CODE

13. ABSTRACT *(Maximum 200 words)*

One of the promising launch concepts that could replace the current Space Shuttle launch system is a two-stage, winged, vertical-takeoff, fully reusable launch vehicle. During the boost phase of ascent, the booster provides propellant for the orbiter engines through a cross-feed system. When the vehicle reaches a Mach number of 3, the booster propellants are depleted and the booster is staged and glides unpowered to a horizontal landing at a launch site runway. Two major design issues for this class of vehicle are the staging maneuver and the booster glideback. For the staging maneuver analysis, a technique was developed that provides for a successful separation of the booster from the orbiter over a wide range of staging angles of attack. A longitudinal flight control system was developed for control of the booster during the staging maneuver. For the booster glideback analysis, a guidance algorithm was developed that successfully guides the booster from the completion of the staging maneuver to a launch site runway while encountering many off-nominal atmospheric, aerodynamic, and staging conditions.

14. SUBJECT TERMS
Launch vehicles; Staging analysis; Booster glideback; Guidance

15. NUMBER OF PAGES
23

16. PRICE CODE
A03

17. SECURITY CLASSIFICATION OF REPORT	18. SECURITY CLASSIFICATION OF THIS PAGE	19. SECURITY CLASSIFICATION OF ABSTRACT	20. LIMITATION OF ABSTRACT
Unclassified	Unclassified		

☆U.S. GOVERNMENT PRINTING OFFICE 1993–728-064/66,018